Spectral Properties of the Signal in Phase-Sensitive Optical Time-Domain Reflectometry With Direct Detection

Xin Lu, Marcelo A. Soto, *Member, OSA*, Li Zhang, and Luc Thévenaz, *Fellow, IEEE, Fellow, OSA*

***Abstract*—The spectral properties of the Rayleigh backscattered traces measured by a phase-sensitive optical time-domain reflectometer (ϕOTDR) with direct detection are theoretically and experimentally analyzed. The spectrum of the measured ϕOTDR signal is found to be strictly dependent on the spectral shape of the probing optical pulse. Furthermore, the visibility, spatial resolution, fading rate, and correlation spectrum of the traces are analyzed using different detection bandwidths. Results point out that the quality of ϕOTDR traces and target spatial resolution are secured only if the electrical bandwidth of the photodetector is broad enough to cover at least 80% of the total power contained in the electrical spectral density function of the measured trace. This means that in the case of using direct detection of the Rayleigh backscattered light induced by rectangular-shaped optical pulses, the minimum bandwidth required for a proper detection of the traces is equal to the reciprocal of the pulse temporal width (which is larger than the pulse spectral width). Although the theoretical analysis and numerical simulations are here experimentally validated for rectangular and sinc-shaped optical pulses, the results and methodology presented in this article can be applied to optimize the direct-detection bandwidth of ϕOTDR sensors using any optical pulse shape.**

***Index Terms*—Fiber optics, optical fiber sensors, optical signal detection, optical time domain reflectometry, Rayleigh scattering.**

I. Introduction

PHASE-SENSITIVE optical time-domain reflectometry (ϕOTDR) is a distributed fiber sensing technique based on coherent Rayleigh scattering, now widely used in intrusion detection, vibration sensing, and distributed temperature or strain measurement [1]–[3]. In a ϕOTDR system, a highly coherent optical pulse is launched into a sensing fiber and the multiple interferences of the Rayleigh backscattered light from distinct scattering centers covered by the optical pulse width are detected. The refractive index of an optical fiber shows minute random variations due to the frozen fluctuating material density. This leads to an interference process that generates a random, but static profile along the fiber, resulting in a temporal trace with a stochastically varying amplitude, which is fully repeatable under entirely identical conditions (i.e., unchanged light spectrum and environmental conditions) [4]. The profile of a ϕOTDR trace carries meaningful information about the local conditions along an optical fiber, and therefore, most of sensing applications are based on the monitoring of the variations of this longitudinal random pattern.

Since this jagged profile contains essential information for ϕOTDR sensing, the temporal trace must be acquired with the best fidelity. Particularly, the ϕOTDR signal shows very fast time-domain oscillations, indicating a rich spectral content. The photoreceiver bandwidth must be therefore large enough to avoid filtering out essential high frequency information. Should the bandwidth be too limited, the randomly varying temporal trace would be longitudinally smoothened, altering the trace signature and leading to a sensing response with reduced sharpness. The requirement for a broadband detection has been pointed out in the case of a rectangular incident pulse and the photodetector bandwidth has been suggested to be several times broader than the optical pulse spectrum [5]. Nevertheless, higher bandwidth means larger noise and this might in turn impair the sensing performance. It is therefore necessary to precisely determine the minimum bandwidth required to secure a trace fidelity good enough for a target spatial resolution.

In this paper, the spectral features of ϕOTDR traces are theoretically and experimentally analyzed. The effects of the photoreceiver bandwidth on the visibility, spatial resolution, fading rate and correlation spectrum of the sensor are also investigated. Results demonstrate that a reduced detection bandwidth can impair the visibility, spatial resolution and fading rate of ϕOTDR traces, as well as broaden the cross-correlation peak of frequency-scanned ϕOTDR systems, impairing the quality and reliability of the measurements. According to this analysis, the photoreceiver bandwidth is assessed to be large enough when containing 80% of the signal power, which

Manuscript received August 13, 2019; revised December 4, 2019 and January 20, 2020; accepted January 30, 2020. Date of publication February 5, 2020; date of current version March 17, 2020. This work was supported in part by the Swiss Commission for Technology and Innovation under Grant 18337.2 PFNM-NM. *(Corresponding author: Xin Lu.)*

X. Lu was with the Institute of Electrical Engineering, Swiss Federal Institute of Technology of Lausanne, CH 1015 Lausanne, Switzerland. He is now with the NORCE Norwegian Research Centre AS, 5892 Bergen, Norway (e-mail: luxin1026@gmail.com).

M. A. Soto was with the Institute of Electrical Engineering, Swiss Federal Institute of Technology of Lausanne, CH 1015 Lausanne, Switzerland. He is now with the Department of Electronic Engineering, Universidad Técnica Federico Santa María, 2390123 Valparaíso, Chile (e-mail: marcelo.sotoh@usm.cl).

L. Zhang and L. Thévenaz are with the Institute of Electrical Engineering, Swiss Federal Institute of Technology of Lausanne, CH 1015 Lausanne, Switzerland (e-mail: li.zhang@epfl.ch; luc.thevenaz@epfl.ch).

Color versions of one or more of the figures in this article are available online at https://ieeexplore.ieee.org.

Digital Object Identifier 10.1109/JLT.2020.2971614

represents the minimum required condition to keep impairments at a negligible level.

II. Theory

The amorphous nature of an optical fiber can be figured out as the coalescence of subwavelength glass domains of random density, resulting in numerous scattering centers, which deflect the incident light in all directions. Thus, while an optical pulse propagates along the fiber, a small fraction of the incident light is back-reflected by the tiny density variations of the material. The optical fields backscattered over the pulse width w - covering a large number of scattering centers - interfere with each other when reaching the detector. Therefore, the reflected light in a ϕOTDR sensor at position z can be seen as the summation of different optical fields, which can be expressed as

$$E\left(z\right) = e^{-\alpha z} \sum_{x=z}^{z+w} P_E\left(x\right) E_0 r\left(x\right) e^{j2\phi(x)}, \tag{1}$$

where α is the fiber attenuation coefficient, $r(x)$ is the amplitude reflection coefficient at position x, E_0 is the peak field amplitude of the optical pulse, $P_E(x)$ represents the normalized pulse amplitude spatial profile, and the optical phase $\phi(z + m\Delta z)$ is the integration of the propagation constant $\beta(z) = 2\pi n(z)\nu/c$ from z to $z + w$ where c is the speed of light in vacuum, $n(z)$ is the local refractive index and ν is the central optical frequency of the incident light. Note that this model assumes a short enough (a few meters) spatial resolution of the ϕOTDR system, so that the fiber loss over the pulse width can be neglected.

Usually, the number of scattering points within the spatial resolution is extremely large due to the subwavelength size of the scattering centers. Thus, the summation in (1) can be replaced by an integration [6], and the reflected field $E(z)$ can be rewritten as

$$E\left(z\right) = \int_0^L P_E\left(x\right) E_0 r\left(x\right) e^{j2\phi(x)} dx = H_E\left(z\right) \otimes P_E\left(z\right), \tag{2}$$

where $\otimes$ denotes a convolution operation, convolving the fiber backscattering impulse response $H_E(z) = E_0 r(z) e^{j2\phi(z)}$ with the interrogating pulse temporal profile [7], L is the fiber length and the fiber loss is neglected for simplicity. Since the refractive index varies randomly along the fiber, the optical phase $\phi(z)$ is a random variable, and $H_E(z)$ is essentially a random function.

According to (2), the reflected light $E(z)$ can be seen as the random function $H_E(z)$ linearly filtered by the incident pulse shape $P_E(z)$ [8]. Thus, the power spectral density (PSD) of the reflected light amplitude can be expressed as the product of the PSD of the random function $H_E(z)$ and the squared modulus of the transfer function of the filter [9]. The PSD of $H_E(z)$ can be obtained by the Fourier transform of the autocorrelation function of $H_E(z)$ [8], and therefore the PSD of the backscattered light can be expressed as:

$$S_E\left(f\right) = S_H \cdot \left|\mathcal{F}\left(P_E\right)\right|^2 = I_0 R_0 \left|\mathcal{F}\left(P_E\right)\right|^2, \tag{3}$$

where f is the frequency, $\mathcal{F}$ denotes the Fourier transform, $S_H = I_0 R_0$ is the spectrally uniform PSD of $H_E(z)$, $I_0 = \langle E_0 E_0^* \rangle$ is the light intensity, $R_0 = \langle r r^* \rangle$ is the power reflection coefficient, $*$ denotes the complex conjugation, and $\langle \cdot \rangle$ represents an ensemble average. Hence, (3) indicates that the spectrum of the reflected light amplitude has the same shape as the spectrum of the incident optical pulse.

Note that the response of a ϕOTDR sensor based on coherent detection is the beat between the backscattered light and a local oscillator (LO), so the measured ϕOTDR trace presents the same spectrum as $S_E(f)$. In other words, (3) actually represents the signal spectrum obtained by coherent detection. A simple way to monitor this spectrum is to directly observe the backscattered light using an optical spectrum analyzer (OSA); alternatively, it can be visualized through the beat signal between $E(z)$ and a LO using an electrical spectrum analyzer (ESA) in the usual power mode.

In the case of direct detection, the spectral components of the reflected light mutually beat on the photodetector. This can be represented as a spectral convolution process. Thus the obtained electrical power spectrum depends on the autoconvolution of $S_E(f)$. A detailed analysis reveals that the expression of the PSD for the reflected light intensity $S_I(f)$ is given by [8], [10]:

$$S_I\left(f\right) = I_0^2 R_0^2 \delta\left(f\right) + S_E\left(f\right) \otimes S_E\left(f\right), \tag{4}$$

where $\delta(f)$ represents the delta function. The second term on the right-hand side of (4) represents the beat of the reflected light with itself. The PSD described by (4) corresponds to the ϕOTDR signal measured by direct detection and can be observed by directly plugging the photo-receiver electrical output into an ESA.

As a result of the presented analysis, we can infer the following interesting properties:

1) the optical power spectrum of the backscattered light is identical to the optical power spectrum of the probing optical pulse;
2) the electrical power spectrum of the ϕOTDR trace measured by direct detection is given by the autoconvolution function of the optical power spectrum of the incident light.

This analysis shows that the spectral content of the detected ϕOTDR trace can significantly differ from that of the probing optical pulse in the case of direct detection. Consequently, unlike other distributed optical fiber sensors, defining the detection bandwidth based only on the optical pulse spectrum might not be completely correct in ϕOTDR systems. The validity of this concept will be challenged numerically and experimentally using two radically different pulse waveforms, of mirrored temporal and spectral properties: rectangular and sinc-shaped pulses.

Rectangular pulses are widely used in ϕOTDR sensing. This pulse shape is expressed as

$$P_E^{rect}\left(t\right) = \begin{cases} 1 & |t| \le \tau_{rect}/2 \\ 0 & |t| > \tau_{rect}/2 \end{cases}, \tag{5}$$

where τ_{rect} represents the temporal full width of the pulse, which is equivalent to the full-width at half-maximum (FWHM) determining the spatial resolution of the ϕOTDR sensor. The corresponding spatial resolution is therefore $c\tau_{rect}/2n$ (equating group and phase velocities for simplicity). The PSD of the backscattered light amplitude can then be easily obtained by

inserting $P_E^{rect}(t)$ in (3), yielding:

$$S_E^{rect}(f) = I_0 R_0 \left| \tau_{rect} \frac{\sin \pi \tau_{rect} f}{\pi \tau_{rect} f} \right|^2. \tag{6}$$

Thus, the spectrum of the ϕOTDR signal measured by coherent detection (or directly visualized using an OSA) should show a sinc squared shape if the incident pulse is rectangular shaped, thus mapping the input pulse spectrum.

Inserting $S_E^{rect}(f)$ in (4), the PSD of the backscattered light intensity as directly delivered by a photodetector is given by

$$S_I^{rect}(f) = I_0^2 R_0^2 \left\{ \delta(f) + \frac{\tau_{rect}}{(\pi f)^2} \left[1 - \frac{\sin(2\pi \tau_{rect} f)}{2\pi \tau_{rect} f} \right] \right\}. \tag{7}$$

The obtained $S_I^{rect}(f)$ turns out to spread over a broader spectrum than $S_E^{rect}(f)$. This suggests that a detection bandwidth broader than the probing pulse spectrum may be required [5], as will be later confirmed.

In contrast, sinc pulses demonstrate a high spectral efficiency, and it may be of interest in ϕOTDR sensing regarding the impact of the spectral content. The sinc pulse temporal envelope is expressed as

$$P_E^{sinc}(t) = \begin{cases} 1 & t = 0 \\ \sin(2\pi t/\tau_{sinc}) / (2\pi t/\tau_{sinc}) & t \neq 0 \end{cases}, \tag{8}$$

where τ_{sinc} is the full width of the pulse, defined as the duration between the two first zeroes. The corresponding spatial resolution from the FWHM is determined as $0.6c\tau_{rect}/2n$. Based on (3) and (4), the power spectra of the backscattered light amplitude and intensity are respectively expressed as

$$S_E^{sinc}(f) = \begin{cases} I_0 R_0 \cdot 2\pi/\tau_{sinc} & |f| \leq \frac{1}{\tau_{sinc}} \\ 0 & |f| > \frac{1}{\tau_{sinc}} \end{cases}, \tag{9}$$

$$S_I^{sinc}(f) = \begin{cases} I_0^2 R_0^2 \left[\delta(f) + \frac{\tau_{sinc}^4}{16} \left(1 - \left| \frac{f \tau_{sinc}}{2} \right| \right) \right] & |f| \leq \frac{2}{\tau_{sinc}} \\ 0 & |f| > \frac{2}{\tau_{sinc}} \end{cases}. \tag{10}$$

According to (9) and (10), while the PSD of the optical Rayleigh amplitude keeps the rectangular spectrum of the input pulse, the PSD of the detected intensity follows a triangular spectral shape, thus being also of strictly bounded finite bandwidth. Therefore, it is possible to acquire the full signal information content by a bandwidth-limited photodetector.

III. Numerical Model

Commonly, an optical fiber is conveniently modelled as a unidimensional medium [1], [6], [11], [12], as shown in Fig. 1, which is composed by uniform scattering segments of length Δz (being of the order of the optical wavelength), and showing randomly varying refractive indices. This can be actually expressed as: $n(z) = n_{ave} + \Delta n(z)$, where $n_{ave} \approx 1.46$ is the average refractive index along the fiber and $\Delta n(z)$ is the local index variation. Based on this definition, (1) can be rewritten as [12]:

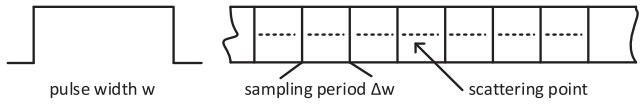

Fig. 1. Unidimensional representation of an optical fiber, modelling the effect of the scattering centers on an incident light pulse [12].

$$E(z) = e^{-\alpha z} \sum_{m=0}^{M} P_E(m) E_0 r(z + m\Delta z) e^{j2\phi(z+m\Delta z)}, \tag{11}$$

where $M = w/\Delta z$ is the number of scattering segments within a sampling interval (here taken as the length covered by the pulse width), $r(z + m\Delta z)$ is the complex reflection coefficient of m^{th} segment, and the optical phase $\phi(z + m\Delta z)$ is the integration of the propagation constant $\beta(z) = 2\pi n(z)\nu/c$ from z to $z + m \cdot \Delta z$.

Due to the large number of scattering centers within the spatial resolution, the refractive index from z to $z + (m-1)\Delta z$ can be approximated by the average index, so that the optical phase in (11) can be expressed as:

$$\phi(z + m\Delta z) \approx 2\pi\nu\Delta z/c \cdot [m \cdot n_{ave} + \Delta n(z + m\Delta z)]. \tag{12}$$

Note that the sensing fiber used in a ϕOTDR system is usually modelled as an ultra-long but weak random grating with arbitrary pitches [13], [14] due to the random refractive index fluctuations along the fiber, and the Rayleigh backscattering can be seen as the light reflected at the interface of two adjacent inhomogeneities. As a result, the reflection coefficient can be straightforwardly obtained using the Fresnel reflection law, assuming the light is normally incident, based on refractive index variations along the fiber. Inserting $r(z + m\Delta z)$ and $\Delta n(z + m\Delta z)$ into (11) and (12), the reflected light $E(z)$ in the ϕOTDR system can be then calculated.

To numerically simulate the reflected light, the refractive index $\Delta n(z)$ at each scattering point is usually randomly generated along the fiber. However, this method is very inefficient because M is a large number, typically of the order of millions. In addition, it is unnecessary to consider every scattering center since the temporal Rayleigh trace is always sampled by the acquisition system at discrete points with a sampling interval Δw, as shown in Fig. 1. Considering the sampling rate used in the ϕOTDR system, each data point contains already information integrated over thousands of scattering centers along the fiber. Hence, the computational workload is here highly reduced by using an equivalent factor $\Delta n'(z_k)$ at each sampled location z_k instead of the index $\Delta n(z)$ [12]. Since the number of scattering centers contributing to each sampling point is still given by all points M inside the pulse, the index variation can be safely assumed to follow a Gaussian distribution as justified by the central limit theorem [6].

The results from this numerical model will be introduced in the next section, in critical comparison with theory and experiment.

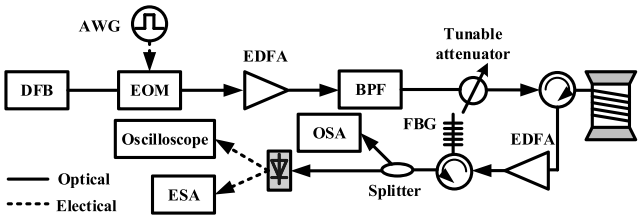

Fig. 2. Implemented experiment setup to acquire the spectral and spatial properties of the ϕOTDR signal.

IV. Experiment and Results

A. Experimental Test Bench

To validate the above analysis, the spectrum of the reflected light originating from Rayleigh backscattering along a 1 km single mode fiber (SMF) is acquired by the standard direct-detection ϕOTDR setup shown in Fig. 2. The light source is a distributed-feedback laser (DFB) with $\sim$1 MHz linewidth at 1550 nm, so presenting a coherent length at least one order of magnitude larger than the pulse width. The continuous-wave laser light is shaped into pulses using an electro-optic modulator (EOM), driven by a 2.3 GS/s arbitrary waveform generator (AWG) to deliver different pulse shapes. In this paper, rectangular and sinc pulses are studied, both with a FWHM of 10 ns, equivalent to a 1 m spatial resolution. The corresponding width τ_{sinc} of the sinc pulse between the two first zeroes is $\sim$ 16 ns. The optical pulse is boosted by an Erbium-doped fiber amplifier (EDFA) and the amplified spontaneous emission (ASE) is suppressed using an optical band-pass filter (BPF). The optical pulse power is leveled using a tunable attenuator to keep it below the critical power for modulation instability [15]. Finally, the pulse is launched into a sensing fiber through a circulator. In order to avoid Fresnel reflections at the fiber ends, which may contaminate the spectrum of the backscattered light, the input of the SMF is carefully spliced to the circulator and the far fiber-end is entwined around a small diameter object. The weak backscattered light is amplified using another EDFA, and a narrow-band (5 GHz) fiber Bragg grating (FBG) is inserted to suppress the ASE. The power spectrum of the light amplitude $S_E(f)$ is visualized using a high-performance OSA with 5 MHz resolution operating in coherent-detection mode. A 1 GHz photodetector converts the backscattered light intensity into a proportional electrical signal. An ESA is employed to observe the electrical spectrum $S_I(f)$ and the temporal Rayleigh trace is acquired by an oscilloscope operating at a sampling rate of 4 GS/s.

B. Simulation Conditions

Temporal ϕOTDR traces for different pulse shapes are numerically calculated using (11) and (12) under preset conditions identical to the experiment. The randomly generated index fluctuations $\Delta n'(z_k)$ obey a zero Gaussian probability distribution with a variance [16]:

$$\sigma_n^2 = 3\lambda^4\alpha/16\pi^3 n^2 D^3 \approx 7.4\times10^{-7}, \tag{13}$$

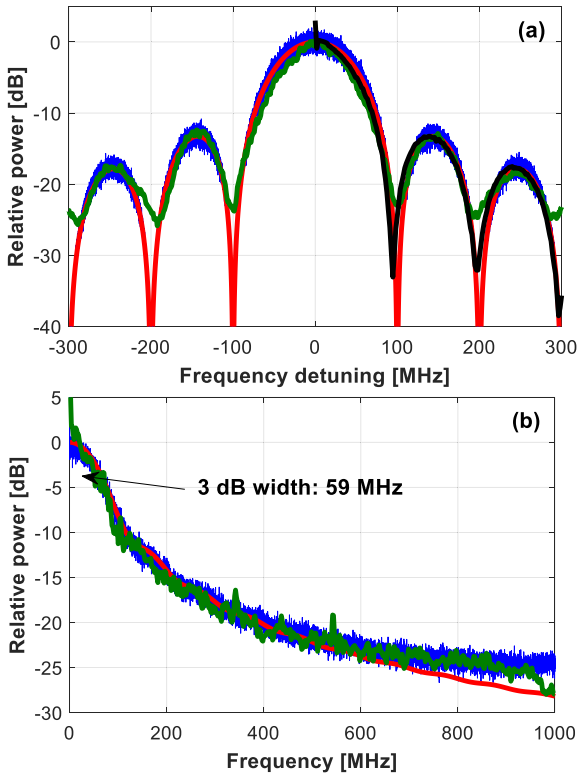

Fig. 3. Comparisons of power spectra of the light (a) amplitude and (b) intensity using 10 ns rectangular pulses, obtained by theoretical analysis (red), numerical simulation (blue), and experiment (green). The black curve represents the measured intensity spectrum of the incident 10 ns rectangular pulse, matching perfectly the backscattered spectrum.

where λ is the wavelength and $D \sim 10$ nm is the correlation length of the refractive index [17]. Then the spectra of the reflected light amplitude and intensity can be obtained from the Fourier transform of the corresponding simulated traces $E(z)$ and $I(z) = |E(z)|^2$. Note that the fiber attenuation is neglected in the simulations because of the short fiber length used in the experiment. In order to perform a reliable comparison with experiments, the digital bandwidth of the simulation is matched to the detection bandwidth of the experimental setup. Thus, the sampling interval Δw is set here at 5 cm (representing a sampling rate of 2 GS/s in simulation and a digital bandwidth of 1 GHz). The number of scattering segments M within each meter of optical fiber considered in the simulations is therefore equal to 20.

C. Results

The spectra obtained theoretically, numerically and experimentally are compared in Fig. 3, for the case of using a rectangular pulse. It can be noticed that the theoretical analysis (red curves) and simulation results (blue curves) agree very well with the experimental results (green curves), thus validating the model assumptions, at least for this important case. In particular, Fig. 3(a) shows that the obtained spectra for the light amplitude $S_E^{rect}(f)$ demonstrate a sinc-squared shape, being the same as the intensity spectrum of the incident rectangular pulse obtained by an ESA (black curve, showing the one-sided electrical

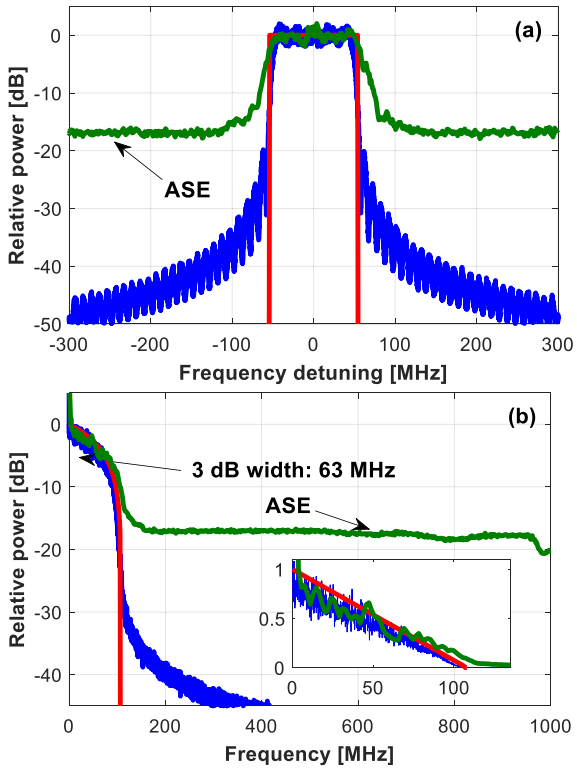

Fig. 4. Comparisons of power spectra of the light (a) amplitude and (b) intensity using 10 ns full width sinc pulses, obtained by theoretical analysis (red), numerical simulation (blue), and experiment (green). Inset shows the relative power in linear scale. ASE from EDFAs contaminates the experimental spectra in regions of very weak frequency components.

spectrum). From the sinc-squared function, the 3 dB spectral width of the rectangular pulse is calculated as $\sim 0.442/\tau_{rect}$ and is measured to be 44.3 MHz in Fig. 3(a) for a 10 ns pulse. In contrast, Fig. 3(b) shows that the intensity spectrum - acquired by direct detection and containing the jagged waveform created by multiple interference - covers a wider frequency range with a 3 dB width of ~59 MHz, being very consistent with the theoretical value $\sim 0.6/\tau_{rect}$ (=60 MHz) [8]. In addition, the simulation of different rectangular pulse widths shows the same relationship between the 3 dB intensity spectrum width and the pulse width. Therefore, the 3 dB bandwidth of the ϕOTDR intensity signal is ~1.4 (= 0.6/0.442) times larger than the rectangular pulse spectrum, showing that the interferences resulting from the coherent reflectometry give rise to faster signal modulations than those merely expected from resolved events along the fiber.

Rectangular pulses are temporally limited and spread over an infinite spectrum. To decisively test the agreement between theory, simulation and experiment, a pulse shape presenting exactly opposed features (unlimited temporal waveform and strictly bounded spectrum) is also formed, in this case using sinc pulses. The Fourier transform of a sinc pulse is a rectangular function, and the 3 dB width of the pulse intensity spectrum is calculated to be 62.5 MHz. Figure 4(a) confirms the expected rectangular shape of the backscattered light amplitude spectrum. The autoconvolution of the rectangular function gives a triangular distribution, so the spectrum of the light intensity shown in Fig. 4(b) linearly decays with frequency, as being clearly confirmed in the inset figure. According to (10), the spectrum must be confined within a finite frequency range, with a 3 dB width identical to that of the rectangular spectrum of the sinc pulse. This is widely confirmed by the experimental results in Fig. 4(a) and 4(b), although being affected by ASE noise introduced by the pre-amplifier, which increases the noise floor of the measurements (green curves). The real spectrum obtained experimentally slightly differs from a perfect rectangle in Fig. 4(a), since the real sinc pulse is of finite duration and outer pulse sidelobes are suppressed. To perform a fair comparison, these sidelobes are also neglected in the simulation, thus accounting for the gradual power decrease outside the pulse spectrum width, as shown in Fig. 4(a) and 4(b).

Figure 3 and 4 show that the ϕOTDR intensity spectrum normally spans over a broader frequency range than the pulse spectrum. This is practically not an issue for coherent detection, since the optical receiver bandwidth must be larger than the frequency difference between the backscattered light and the local oscillator, which is usually several times broader than the optical pulse spectrum. Therefore, the photodetector bandwidth in coherent detection can safely be considered large enough for a ϕOTDR signal. However, the detection bandwidth required for a direct-detection ϕOTDR system still needs to be determined to secure a given spatial resolution and a good ϕOTDR trace quality. This will be addressed in the next section.

V. Impact of Photo-Detection Bandwidth

A. Trace Visibility

The impact of the photodetector bandwidth can be simply analyzed by post-processing using the internal digital filter of the oscilloscope. As stated before, the use of a limited bandwidth smooths the jagged shape of the ϕOTDR traces, thus lowering their contrast, or visibility, commonly defined as $V = (I_{\max} - I_{\min})/(I_{\max} + I_{\min})$. Visibility is an essential factor to quantify the quality of ϕOTDR traces. Figure 5(a) shows the visibility evaluated from experimental data over a moving window of 10 m along a 1 km fiber, when using 10 ns rectangular pulse. According to its definition, the visibility describes the trace contrast within a certain fiber section, and is highly dependent on $I_{\min}$. This means that the visibility equals to 1 when $I_{\min} = 0$, regardless of the value of $I_{\max}$. The smoothing effect of narrow detection bandwidths is equivalent to a longitudinal average of the trace over a certain distance, resulting in an increased $I_{\min}$ value. Consequently, it can be observed in Fig. 5(a) that the use of a reduced bandwidth results in a low mean visibility, which leads to a poor trace quality, since informative high frequency components are filtered out by the limited bandwidth. In addition, the minimum intensity $I_{\min}$ turns out to be significantly offset at some fiber positions, leading to a comparatively low local visibility and resulting in a larger variability of the visibility along the trace, as shown in Fig. 5(a). As the detection bandwidth narrows, more fiber sections exhibit low visibility, resulting in a mean visibility that reduces while its longitudinal variability increases. Note that the visibility will be very low over the whole fiber when the

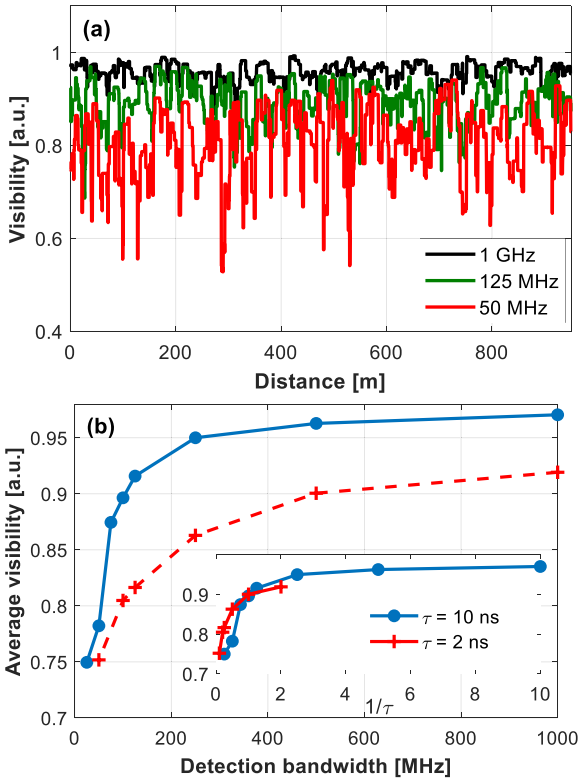

Fig. 5. Impact of detection bandwidth on (a) the visibility along the fiber with $\tau = 10$ ns pulse and (b) the averaged visibility, for the case of rectangular pulse.

bandwidth is very narrow, so that the longitudinal fluctuations of the visibility becomes small again in this extreme case.

This aspect is presented more clearly in Fig. 5(b), which shows the average visibility over the fiber as a function of the detection bandwidth for 10 ns and 2 ns rectangular pulses. As expected, keeping the same bandwidth, the visibility of the ϕOTDR trace obtained by a 10 ns pulse is always higher than the one obtained with a 2 ns pulse, due to the narrower spectral width of the probing pulse. The visibility however decreases as the bandwidth becomes smaller in the two cases, leading to poor performance (e.g., due to low sensitivity) and resulting in large measurand errors [3] and/or degraded spatial accuracy [1]. Large bandwidths however introduce more noise, which impairs the whole sensing performance. This behavior verifies the existence of a clear tradeoff between the detection bandwidth and the sensing performance. The relation between the visibility and bandwidth is further analyzed in the inset of Fig. 5(b), where the bandwidth is normalized to $1/\tau_{rect}$ for a better interpretation. Clearly, the visibilities in both cases decrease dramatically when the normalized bandwidth is below 1, i.e., when the visibility reaches the value of 0.9, which can be defined as a visibility threshold. Therefore the corresponding bandwidth threshold turns out to be exactly $1/\tau_{rect}$. Note however that the visibility of ϕOTDR traces may also depend on other factors, such as the presence of modulation instability [15] and the degree of coherence of the laser [18]. Hence, the visibility threshold may vary under non-optimized experimental conditions, but its corresponding bandwidth should always be $1/\tau_{rect}$.

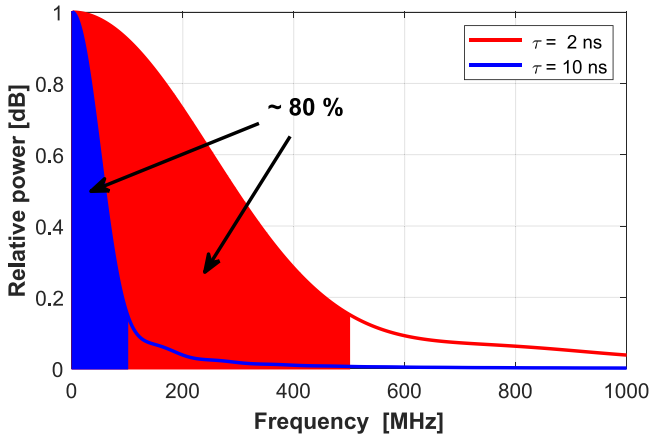

Fig. 6. Impact of detection bandwidth on the received power ratio over the whole spectrum, in the case of rectangular incident pulses.

B. Detected Signal Power

As described before, the inset of Fig. 5(b) points out that the detection bandwidth must be at least $1/\tau_{rect}$ to secure a good trace visibility and good correlation features. However, due to the theoretically unlimited bandwidth of rectangular pulses and the resulting Rayleigh backscattering intensity, this threshold bandwidth results in a reduction of the received signal power. To illustrate this, Fig. 6 shows colored areas that represent the integrated power that is received within a bandwidth of $1/\tau_{rect}$ for 10 ns and 2 ns pulses, respectively. Note that this integrated power represents 80% of the total signal power, indicating that this fraction of the total power defines the minimum power required to be detected to secure good quality traces. To determine this bandwidth $f_{80\%}$ analytically for any arbitrary pulse width, the intensity spectrum $S_I(f)$ integrated between $\pm f_{80\%}$ must be equaled to 80% of the integration over the whole spectrum. Unfortunately, this results in a transcendental equation that has no analytic solution. However, numerical solutions using rectangular pulses of different widths τ_{rect} have been analyzed, concluding and demonstrating that a detection bandwidth of $1/\tau_{rect}$ secures that 80% of the signal power is indeed measured.

C. Spatial Resolution

The impact of the reduced visibility demonstrated in Fig. 5 as a result of a limited detection bandwidth is also evaluated by the temporal autocorrelation of traces measured with different bandwidths. Figure 7 shows that the temporal correlation peak becomes wider as the detection bandwidth decreases below a given threshold. This broadening effect is actually more visible when the bandwidth is reduced below 100 MHz, as the average visibility drops below 0.9 according to Fig. 5(b). This is in good agreement with the expected minimum bandwidth defined by the reciprocal of the pulse temporal width.

The temporal width of the autocorrelation function actually determines the spatial resolution of the sensor (note that only half of the temporal autocorrelation function is shown here). While unaffected ϕOTDR traces are expected to be correlated only within the pulse width duration (assuming unlimited bandwidth)

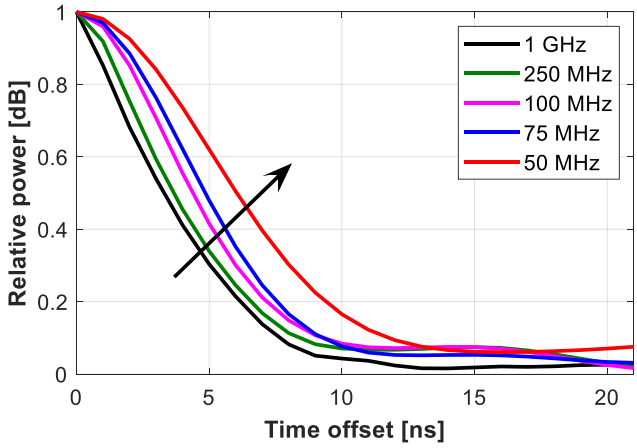

Fig. 7. Impact of detection bandwidth on the spatial resolution of the sensor, quantified by the temporal autocorrelation of the traces for different detection bandwidths, in the case of rectangular incident pulses.

[19], [20], the presence of broadening in the temporal correlation peak indicates a clear spatial resolution impairment when using reduced detection bandwidth.

Complementary to previous results based on rectangular pulses, the trace visibility and spatial resolution impairment are also investigated in the case of sinc-shaped pulses. In this case, a sinc pulse with a FWHM of 10 ns is used to obtain ϕOTDR traces with 1 m spatial resolution. According to (10), the bandwidth required to collect 80% of the signal spectrum can be calculated for a sinc pulse as

$$\int_{-f_{80\%}}^{f_{80\%}} \frac{\tau_{sinc}^4}{16}\left(1-\left|\frac{x\tau_{sinc}}{2}\right|\right)dx = \frac{4}{5}\int_{-\frac{2}{\tau_{sinc}}}^{\frac{2}{\tau_{sinc}}} \frac{\tau_{sinc}^4}{16}\left(1-\left|\frac{x\tau_{sinc}}{2}\right|\right)dx \qquad (14)$$

where the delta function is simply neglected in the integration. The corresponding bandwidth $f_{80\%}$ is $\sim 1.1/\tau_{sinc}$. Thus, the minimum detection bandwidth to achieve 1 m resolution is ~70 MHz, as shown in the inset of Fig. 8(a). The main graph in the figure shows the dependence of the average visibility on the bandwidth. Based on (10) and Fig. 4(b), the ϕOTDR signal is strictly confined within the frequency range from 0 to $2/\tau_{sinc}$, so no electrical signal components are present beyond $2/\tau_{sinc}$. As a result, the visibility only changes negligibly when the bandwidth exceeds 250 MHz. A small visibility reduction is observed when the detection bandwidth is decreased from 250 MHz down to 125 MHz (2/16 ns) presumably due to the spectral broadening caused by the imperfect sinc pulse shape. The visibility reduces to 0.9 for a bandwidth of 75 MHz, not far from the 80% spectral collection rule (obtained at ~70 MHz). In addition, a large correlation peak broadening, indicating a decaying spatial resolution, is observed when the bandwidth is reduced below 100 MHz, as shown in Fig. 8(b), which is also in good agreement with the theoretical analysis presented above.

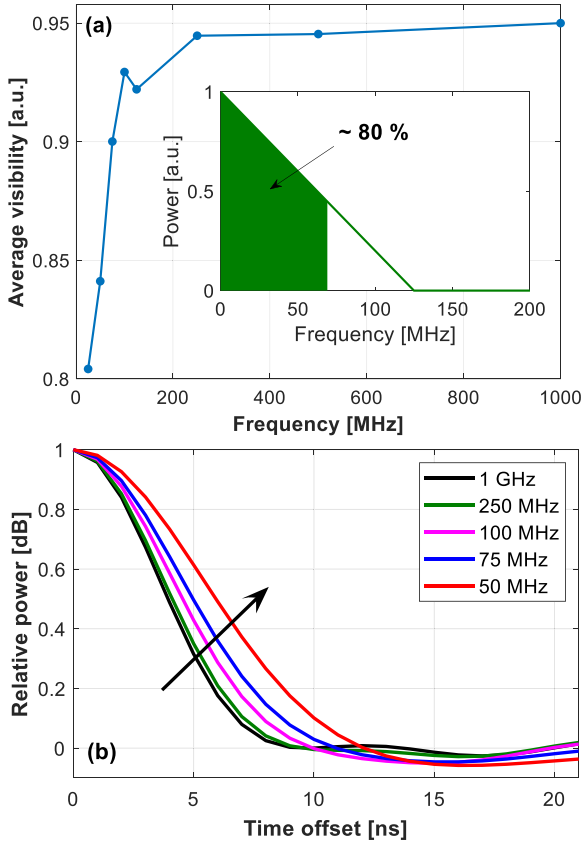

Fig. 8. Impact of detection bandwidth on (a) average visibility and (b) temporal autocorrelation of the ϕOTDR traces obtained for different detection bandwidth when using sinc-shaped incident pulse with a zero-crossing width of 16 ns.

D. Fading Rate

In addition to the spatial resolution impairments, the smoothening effect on the traces resulting from a limited photodetection bandwidth also affects other sensing performance parameters, especially related to the quality and reliability of the measurements. Actually, the reduction of visibility results on a smooth trace with a reduced number of fading points, having an impact on the sensitivity of the sensor and on the quality of the measurand. In order to evaluate the impact of detection bandwidth on the fading rate, the proportion of sampled points in which the signal amplitude falls below the 20% of the mean signal level is calculated. This level is actually here considered as a threshold value, beyond which the extraction of the measurand information is severely impaired, resulting in detection errors and false alarms. Figure 9 shows the fading rate calculated over ϕOTDR traces as a function of the detection bandwidth. Results evidently show how the use of a reduced bandwidth decreases the fading rate, especially at detection bandwidths below 100 MHz, as theoretically expected. This is clearly linked to the reduced visibility of the traces resulting from limited detection bandwidth, which leads in a loss of sensitivity and causing potential detection errors and false alarms.

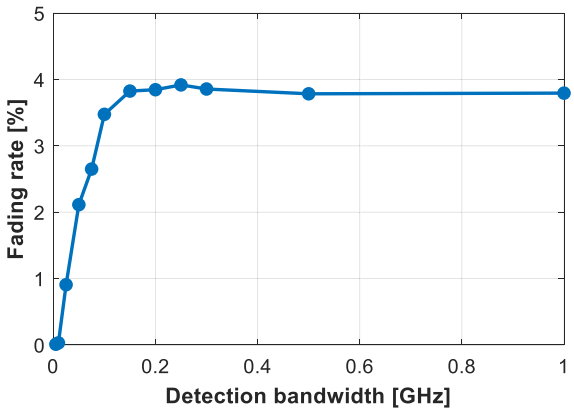

Fig. 9. Impact of detection bandwidth on the number of fading points for a direct-detection ϕOTDR sensor with 10 ns rectangular pulses.

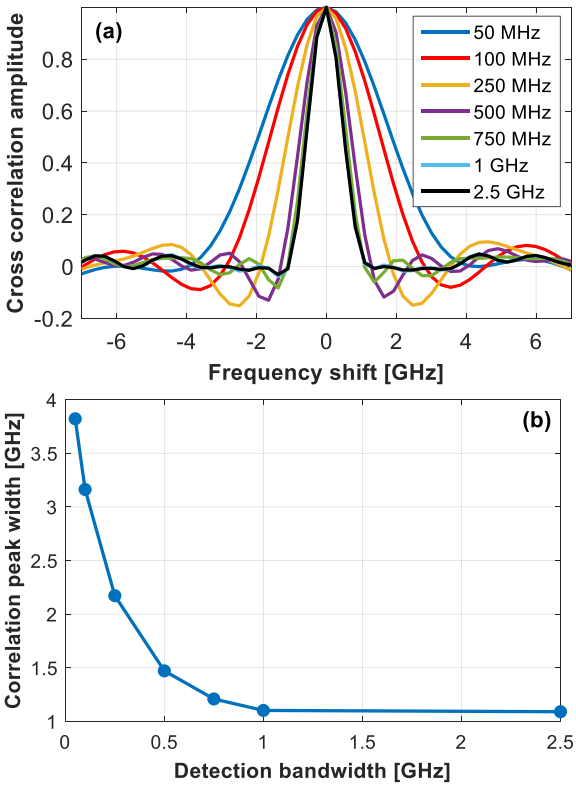

Fig. 10. Impact of detection bandwidth on the spectral width of the cross-correlation function for a direct-detection ϕOTDR sensor with 1 ns rectangular pulses. (a) Experimental cross-correlation spectrum for different bandwidths. (b) Spectral FWHM of the correlation peak as a function of the detection bandwidth, demonstrating that the lowest required bandwidth matches the value of $1/\tau_{rect} = 1$ GHz.

E. Correlation Function and Measurand Resolution

By tuning the laser chip temperature in the setup of Fig. 2, it is possible to perform direct-detection ϕOTDR sensing based on frequency scanning [21], [22]. Using a rectangular probing pulse of 1 ns (i.e., 10 cm spatial resolution), the impact of detection bandwidth on the performance of the sensor is here investigated. An oscilloscope and a photodetector with larger bandwidths are here used to achieve such a spatial resolution and to analyze the effect of detection bandwidths up to 2.5 GHz. Environmental information is retrieved in this case by performing measurements based on a frequency scanning and comparing these actual measurements with a reference. A cross-correlation between measurement and reference spectra is carried out at each fiber location. Fig. 10(a) shows the cross-correlation spectra obtained with no environmental variations (i.e., resulting in a cross-correlation peak centered at a frequency shift equal to zero) for different detection bandwidths. Results show that as the detection bandwidth reduces, the correlation peak broadens considerably, especially for bandwidths below 1 GHz. This is more evident in Fig. 10(b), which shows the actual FWHM of the cross-correlation peak as a function of the detection bandwidth. Note that the use of a shorter pulse width in this case (i.e., 1 ns pulse instead of 10 ns pulse, as in the previous analysis) can enable to verify that the bandwidth limitation predicted by our theory scales up linearly, resulting in a $1/\tau_{rect}$ bandwidth equal to 1 GHz (instead of 100 MHz as for 10 ns pulses). Considering that the peak frequency is normally estimated by quadratic fitting, the induced broadening is expected to enlarge the frequency uncertainty, thus impairing the measurand resolution with a square-root dependence on the peak width [23].

VI. Conclusion

In this paper, the spectral properties of the ϕOTDR signal have been analyzed theoretically and experimentally for different probing pulse shapes. The support of a numerical approach has been used to validate the model assumptions by simulating the ϕOTDR signal in temporal and spectral domains for arbitrary incident pulse shapes. The minimum detection bandwidth required to acquire ϕOTDR traces and maintain high visibility has been investigated and experimentally validated in the case of rectangular and sinc pulses. Based on the analysis of visibility, spatial resolution, fading rate and correlation spectrum of the traces, at least 80% of the signal power spectrum must be received to secure ϕOTDR traces with a given spatial resolution and to allow the proper retrieval of information from the interferences forming the traces. In the canonic case of a rectangular probing pulse, the minimum required detection bandwidth turns out to be the exact reciprocal of the pulse width $1/\tau_{rect}$. It must be noted that this value is much larger ($\sim$1.4 times) than the required bandwidth to resolve an equivalent spatial resolution in traditional distributed fiber sensors, such incoherent Rayleigh, Raman and Brillouin OTDRs. This comes from the fact that the interference pattern within the pulse width in coherent Rayleigh reflectometry shows an average periodicity shorter than the pulse width, imposing higher detection bandwidth requirements. Although the analysis has been here carried out for rectangular and sinc shaped pulses, the proposed analysis can be applied to any arbitrary pulse shapes. The obtained results and proposed methodology are expected to provide guidelines for designing ϕOTDR sensors with optimal detection bandwidth.

REFERENCES

[1] J. Park and H. F. Taylor, "Fiber optic intrusion sensor using coherent optical time domain reflectometer," *Jpn. J. Appl. Phys.*, vol. 42, pp. 3481–3482, Jun. 2003.

[2] R. Zinsou, X. Liu, Y. Wang, J. Zhang, Y. Wang, and B. Jin, "Recent progress in the performance enhancement of phase-sensitive OTDR vibration sensing systems," *Sensors*, vol. 19, Apr. 2019, Art. no. 1709.

[3] X. Lu, M. A. Soto, and L. Thévenaz, "Temperature-strain discrimination in distributed optical fiber sensing using phase-sensitive optical time-domain reflectometry," *Opt. Express*, vol. 25, no. 14, pp. 16059–16071, Jul. 2017.

[4] M. Imahama, Y. Koyamada, and K. Hogari, "Restorability of Rayleigh backscatter traces measured by coherent OTDR with precisely frequency-controlled light source," *IEICE Trans. Commun.*, vol. E91, no. 4, pp. 1243–1246, Mar. 2010.

[5] H. F. Martins, S. Martin-Lopez, P. Corredera, M. L. Filograno, O. Frazão, and M. González-Herráez, "Coherent noise reduction in high visibility phase-sensitive optical time domain reflectometer for distributed sensing of ultrasonic waves," *J. Lightw. Technol.*, vol. 31, no. 23, pp. 3631–3637, Dec. 2013.

[6] J. Zhou, Z. Pan, Q. Ye, H. Cai, R. Qu, and Z. Fang, "Characteristics and explanations of interference fading of a ϕ-OTDR with a multi-frequency source," *J. Lightw. Technol.*, vol. 31, no. 17, pp. 2947–2954, Sep. 2013.

[7] Y. Wu, Z. Wang, J. Xiong, J. Jiang, S. Lin, and Y. Chen, "Interference fading elimination with single rectangular pulse in ϕ-OTDR," *J. Lightw. Technol.*, vol. 37, no. 13, pp. 3381–3387, Jul. 2019.

[8] A. E. Alekseev, V. S. Vdovenko, B. G. Gorshkov, V. T. Potapov, and D. E. Simikin, "A phase-sensitive optical time-domain reflectometer with dual-pulse diverse frequency probe signal," *Laser Phys.*, vol. 25, Apr. 2015, Art. no. 065101.

[9] J. W. Goodman, "Random process," in *Statistical Optics*, 2nd ed., New York, USA: Wiley, 2000, pp. 60–115.

[10] P. Gysel and R. K. Staubli, "Spectral properties of Rayleigh backscattered light from single-mode fibers caused by a modulated probe signal," *J. Lightw. Technol.*, vol. 8, no. 12, pp. 1792–1798, Dec. 1990.

[11] A. Masoudi and T. P. Newson, "Analysis of distributed optical fibre acoustic sensors through numerical modelling," *Opt. Express*, vol. 25, no. 25, pp. 32021–32040, Dec. 2017.

[12] X. Lu, M. A. Soto, and L. Thévenaz, "Optimal detection bandwidth for phase-sensitive optical time-domain reflectometry," *Proc. SPIE*, vol. 9916, 2016, Art. no. 99162N.

[13] M. Froggatt and J. Moore, "High-spatial-resolution distributed strain measurement in optical fiber with Rayleigh scatter," *Appl. Opt.*, vol. 37, no. 10, pp. 1735–1740, Apr. 1998.

[14] X. Lu, M. A. Soto, and L. Thévenaz, "Impact of the fiber coating on the temperature response of distributed optical fiber sensors at cryogenic ranges," *J. Lightw. Technol.*, vol. 36, no. 4, pp. 961–967, Feb. 2018.

[15] H. F. Martins, S. Martin-Lopez, P. Corredera, P. Salgado, O. Frazão, and M. González-Herráez, "Modulation instability-induced fading in phase-sensitive optical time-domain reflectometry," *Opt. Lett.*, vol. 38, no. 6, pp. 872–874, Mar. 2013.

[16] D. Marcuse, "Fundamentals," in *Principles of Optical Fiber Measurements*, New York, USE: Academic Press, 1981, pp. 11–68.

[17] A. Yariv, H. Blauvelt, and S. Wu, "A reduction of interferometric phase-to-intensity conversion noise in fiber links by large index phase modulation of the optical beam," *J. Lightw. Technol.*, vol. 10, no. 7, pp. 978–981, Jul. 1992.

[18] A. E. Alekseev, Y. A. Tezadov, and V. T. Potapov, "The influence of the degree of coherence of a semiconductor laser on the statistic of the backscattered intensity in a single-mode optical fiber," *J. Commun. Technol. Electron*, vol. 56, no. 12, pp. 1490–1498, 2011.

[19] L. B. Liokumovich, N. A. Ushakov, O. I. Kotov, M. A. Bisyarin, and A. H. Hartog, "Fundamentals of optical fiber sensing schemes based on coherent optical time domain reflectometry: signal model under static fiber conditions," *J. Lightw. Technol.*, vol. 33, no. 17, pp. 3660–3671, Sep. 2015.

[20] M. D. Mermelstein, R. Posey, G. A. Johnson, and S. T. Vohra, "Rayleigh scattering optical frequency correlation in a single-mode optical fiber," *Opt. Lett.*, vol. 26, no. 2, pp. 58–60, Jul. 2001.

[21] Y. Koyamada, M. Imahama, K. Kubota, and K. Hogari, "Fiber-optic distributed strain and temperature sensing with very high measurand resolution over long range using coherent OTDR," *J. Lightw. Technol.*, vol. 27, no. 9, pp. 1142–1146, May 2009.

[22] L. Zhang, L. D. Costa, Z. Yang, M. A. Soto, M. Gonzalez-Herráez, and L. Thévenaz, "Analysis and reduction of large errors in Rayleigh-based distributed sensor," *J. Lightw. Technol.*, vol. 37, no. 18, pp. 4710–4719, Sep. 2019.

[23] M. A. Soto and Luc Thévenaz, "Modeling and evaluating the performance of Brillouin distributed optical fiber sensors," *Opt. Express*, vol. 21, no. 25, pp. 31347–31366, Dec. 2013.

Xin Lu received the M.Sc. degree in optical engineering from the University of Electronic Science and Technology of China, Chengdu, China, in 2011 and the Ph.D. degree in electrical engineering from the Swiss Federal Institute of Technology of Lausanne, Lausanne, Switzerland, in 2016. From November 2016 to November 2017, he was with the Institute for Astronomy, Swiss Federal Institute of Technology, Zurich, Switzerland, as a Postdoctoral Researcher. He is currently a Scientist with NORCE Norwegian Research Center AS, Bergen, Norway, working on distributed acoustic and chemical sensing. His main research interests include distributed fiber sensing, nonlinearities in optical fibers, adaptive optics, and high-contrast imaging.

Marcelo A. Soto received the M.Sc. degree in electronic engineering from Universidad Técnica Federico Santa María, Valparaíso, Chile, in 2005 and the Ph.D. degree in telecommunications from the Scuola Superiore Sant Anna, Pisa, Italy, in 2011. During 2010–2011, he was a Research Fellow with Scuola Sant'Anna, where he worked on distributed optical fiber sensors based on Raman and Brillouin scattering. Later, he was a Postdoctoral Researcher with the EPFL Swiss Federal Institute of Technology of Lausanne, Switzerland, where he worked on high-performance Brillouin and Rayleigh distributed fiber sensing, nonlinear fiber optics, optical signal processing, and optical Nyquist pulse generation. Since March 2018, he has been a Tenure-Track Assistant Professor with Universidad Técnica Federico. He also has an invited position as one of the "100 distinguished invited professors" with Guangzhou University in China. He is an author or coauthor of more than 160 scientific publications in international refereed journals and conferences, three book chapters, and eight patents in the fields of optical communications and optical fiber sensing. He is member of the Optical Society of America and is in the Board of Reviewers of major international journals in photonics.

Li Zhang received the B.Sc. degree in optical information science and technology from the Ocean University of China, Qingdao, China, in 2013 and the M.Sc. degree in optical engineering from the University of Electronic Science and Technology of China, Chengdu, China, in 2016. In 2016, she joined the Group for Fibre Optics, Swiss Federal Institute of Technology of Lausanne, Switzerland, as a Doctoral Research Assistant. Her main research interest is focused on distributed optical fiber sensing based on Rayleigh scattering.

Luc Thévenaz (Fellow, IEEE) received the M.Sc. and Ph.D. degrees in physics from the University of Geneva, Geneva, Switzerland, in 1982 and 1988, respectively. In 1988, he joined the Ecole Polytechnique Fédérale de Lausanne (EPFL), Switzerland, where he currently leads a research group (Group for Fibre Optics) involved in photonics, namely fiber optics and optical sensing. Research topics include Brillouin-scattering fiber sensors, slow and fast light, nonlinear fiber optics, and laser applications in gases. He achieved with his collaborators the first experimental demonstration of optically controlled slow and fast light in optical fibers, realized at ambient temperature and operating at any wavelength since based on stimulated Brillouin scattering. He also contributed to the development of Brillouin distributed fiber sensing by proposing innovative concepts pushing beyond barriers. During his career, he stayed with Stanford University, Korea Advanced Institute of Science and Technology, Tel Aviv University, University of Sydney, and Polytechnic University of Valencia. In 2000, he cofounded the company Omnisens that is developing and commercializing advanced photonic instrumentation based on distributed fiber sensing. He chaired the International Conference on Optical Fiber Sensors, is a co-Executive Editor-in-Chief for *Nature Light: Science & Applications*, and is an OSA Fellow.